AD-A132 179 AN EXPLORATORY STUDY OF A THREE-DIMENSIONAL SHOCK WAVE 1/1
BOUNDARY LAYER INT..(U) PRINCETON UNIV N J DEPT OF
AEROSPACE AND MECHANICAL SCIENCES.. B OSKAM ET AL.
UNCLASSIFIED MAY 75 PUAMS-1227 F33615-73-C-3133 F/G 20/4 NL

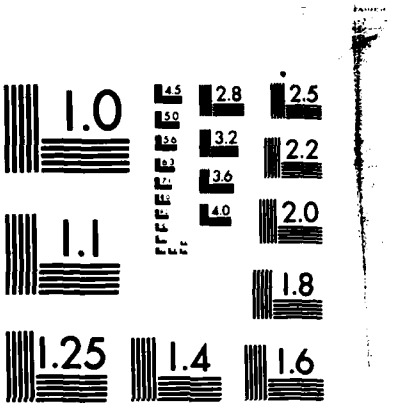

Princeton University

AN EXPLORATORY STUDY OF A THREE-DIMENSIONAL SHOCK WAVE BOUNDARY LAYER INTERACTION AT MACH 3

by

B. Oskam, I. E. Vas and S. M. Bogdonoff

Report 1227

Department of Aerospace and Mechanical Sciences

2

AN EXPLORATORY STUDY OF A THREE-DIMENSIONAL SHOCK WAVE BOUNDARY LAYER INTERACTION AT MACH 3

by

B. Oskam, I. E. Vas and S. M. Bogdonoff

Report 1227

Presented at the AGARD Symposium on Flow Separation
Göttingen, Germany

May 1975

F33615-73-C-3133

AN EXPLORATORY STUDY OF A THREE-DIMENSIONAL SHOCK WAVE BOUNDARY LAYER INTERACTION AT MACH 3

by

B. Oskam, I. E. Vas and S. M. Bogdonoff
Princeton University
Princeton, New Jersey 08540, U.S.A.

SUMMARY

An exploratory experimental investigation has been carried out on the three dimensional flow fields caused by the interaction of oblique shock waves and a planar turbulent boundary layer. The study was performed at a free stream Mach number of 2.95, a Reynolds number per inch of 1.6×10^6 and near adiabatic wall conditions. The interaction was studied on two experimental configurations having different initial boundary layer thicknesses ($\delta \approx 0.13$ and 0.55 inches). Both surface measurements as well as complete flow field surveys were performed.

The main contributions of the present investigation are two experimentally derived flow field models for shock generator angles of 4^o and 10^o. Based upon both static pressure and surface flow patterns, as well as heat transfer data, the interaction region can be characterized as quasi-two-dimensional along the shock direction in the region studied.

A critical examination of the occurance of "ordinary" flow separation and its character, as applied to the present problem, was carried out. It was concluded that McCabe's criterion, as used by the previous investigators, is not a sufficient condition to determine the onset of flow separation.

LIST OF SYMBOLS

a	local speed of sound
C_p	specific heat at constant pressure
$C_f = \frac{\tau_w}{\frac{1}{2}\rho_1 u_1^2}$	local skin friction coefficient
$C_h = \frac{q_c}{\rho_1 u_1 C_p (T_w - T_{aw})}$	local heat transfer coefficient
$M = \frac{\sqrt{u^2+v^2}}{a}$	Mach number
p	static pressure
q_c	convective heat transfer
$Re_\delta = \frac{\rho_1 u_1 \delta}{\mu_1}$	Reynolds number based on δ
t	time
T	temperature
T_{aw}	adiabatic wall temperature
u,v,w	velocity components in X, Y and Z directions
u_{inc}	u-velocity transformed by van Driest transformation of Ref. 8
$u_\tau = \sqrt{\frac{\tau_w}{\rho_w}}$	skin friction velocity
X	coordinate parallel to tunnel axis measured from leading edge of shock generator
X_s	coordinate parallel to X-axis measured from calculated shock position
Y	coordinate normal to X-axis in plane of the test surface measured from leading edge of shock generator
Z	coordinate normal to X- and Y-axis measured from test surface
$\alpha = \arctan(\frac{v}{u})$	yaw angle
α_o	angle between oil line and X-axis
$\alpha_{o_{max}}$	maximum of α_o for fixed shock generator angle
α_G	effective shock generator angle measured with respect to X-axis
$\beta = \arctan(\frac{w}{u})$	pitch angle
δ_1	boundary layer thickness at $(X_s = -\Delta X)$ for fixed Y
δ_{ave}	average δ_1 (as defined in Section 4.3)
δ^*	displacement thickness
ΔX	upstream extent of interaction
θ	momentum defect thickness
μ	viscosity
ρ	density
τ_w	surface shearing stress
ν	kinematic viscosity

Subscripts

1	as in free stream ahead of interaction
2	uniform conditions behind shock wave as calculated from oblique shock theory

Subscripts (Cont'd)

w	wall conditions
vD	van Driest

Superscripted variables

$\bar{p}$	corresponds to $\frac{p}{p_1}$
$\bar{u}$, $\bar{v}$, $\bar{w}$	corresponds to $\frac{u}{u_1}$, $\frac{v}{u_1}$, $\frac{w}{u_1}$
$\bar{X_s}$, $\bar{Z}$	corresponds to $\frac{X_s}{\delta_1}$, $\frac{Z}{\delta_1}$

1. INTRODUCTION

Since the early studies of supersonic flow, there has been continued research on the problems of the interaction of shock waves and turbulent boundary layers. These studies have been concerned with geometries where the pressure gradients were imposed in the streamwise direction, resulting in planar, two-dimensional flows. In most cases of practical importance, there are probably significant three-dimensional effects. In nominally two-dimensional flows this three-dimensionality is associated with end or corner restraints and involves gradients in flow properties in all three directions. However, there is a large class of three-dimensional flows which contain one particular direction along which flow properties vary only slowly. In this class of shock wave/boundary layer interactions, one might expect a quasi-two-dimensional character and therefore a simplification over the full three-dimensional problem.

The study presented herein deals with such a quasi-two-dimensional interaction between an oblique shock wave and the turbulent boundary layer on a surface parallel to the stream but perpendicular to the plane of the shock. Interactions of this kind are found, for example, on the sidewalls of rectangular supersonic air intakes or oblique shock diffusers. The geometry produces both streamwise as well as transverse pressure gradients resulting in significant cross flows in the boundary layer. These complex three-dimensional flows have been the subject of only a few studies, primarily because of the experimental difficulty involved in the full resolution of the flow phenomena. McCabe[1] and Lowrie[2] have studied the problem both experimentally and theoretically. McCabe presented an approximate inviscid theory, based on vorticity arguments, which relates the limiting surface streamline angle to the shock conditions. This theory incorporates some fairly sweeping assumptions, which result in an oversimplification of the physical situation and therefore severely limits the understanding that can be gained from it. A more complicated and also more realistic treatment has been given by Lowrie. His analysis is primarily based on the argument that the pressure gradient term in the momentum equation is much larger than the shear stress term and, consequently, the problem is treated as inviscid rotational fluid flow. The development of cross flows within the boundary layer can be predicted in this way, but only in an initial region of the interaction where the pressure gradient is indeed the dominant effect. It should be noted that Lowrie assumed constant static pressure in the direction normal to the wall in both his theory and his experiments. He reported that boundary layer profiles that showed a static pressure variation of more than 5% were discarded.

Token[3] and Neumann[4] have concentrated on surface heat transfer as it is most important for direct practical applications. Although McCabe, Lowrie and Token provide a large amount of information about the three-dimensional interaction of an oblique shock wave with a turbulent boundary layer each of these studies leaves a significant part of the phenomenon unresolved.

The present study involves the same general problem as examined by the previous investigators but with a somewhat different objective; to examine, in a well-defined experimental set-up, the complete flow field of the interaction and to directly connect this flow field with the surface phenomena. The goal is to provide a better understanding of the phenomena by considering many different aspects of the complete interaction and to form a framework for future experimental and theoretical studies.

Variable strength shock waves, at a Mach number of 2.95, interacting with a high Reynolds number turbulent boundary layer were the general framework of the experimental program. The shock interaction studied was at some distance from the shock generator to try to determine the characteristics of the interaction in a region not directly influenced by the streamwise corner formed by the shock generator and the test surface. Major concentration was on the study of the interaction using one relatively thick turbulent boundary layer (Model 1), but the scope of the study was extended to a much thinner turbulent boundary layer (Model 2) to examine scaling effects.

Special attention was paid to the phenomenon of flow separation in three dimensions. It should be noted that a unique characteristic of three-dimensional flow is that it can separate from the surface without the mean surface shear stress becoming zero. This type of flow separation, known as ordinary separation, has to be distinguished from singular separation whose principal characteristic is that the mean wall shear stress is zero at the separation point (e.g., the separation in planar, two-dimensional flows is singular). Previous investigators of the present problem have indicated the occurance of ordinary separation along a line defined on the basis of surface oil flow patterns. The present investigation examines this ordinary separation on the basis of both surface phenomena as well as flow field measurements.

2. EXPERIMENTAL PROGRAM

2.1 Geometrical Arrangements

A schematic of the experimental configuration, showing the region of detailed measurement, is presented in Fig. 1. The oblique shock was generated by a variable angle shock generator which spanned the tunnel between top and bottom wall. As noted, the region of study extends upstream of the interaction to establish the incoming boundary layer characteristics. The test region does not extend to the shock generator, and is limited in extent by the expansion from the trailing edge of the shock generator and the reflection of the shock from the wall opposite to the shock generator. In any such experimental set-up, extraneous interference effects from the boundaries of the region of study can be expected and great effort

was made to evaluate these effects. The length of the shock generator was made long enough so that the expansion from the trailing edge did not interfere with the region of study and a detailed examination was made of the region of influence of the reflection of the shock wave from the opposite wall.

One of the key parameters of the study is the effect of shock strength which was varied by changing the deflection angle of the shock generator. Two configurations of this general format (Fig. 2) were studied in detail; their main difference was the thickness of the boundary layer coming into the interaction region. Most of the studies were carried out on Model 1, because the relatively thick turbulent boundary layer allowed high resolution measurements to be made throughout the interaction region. The configuration of Model 2 incorporates a much smaller incoming boundary layer thickness and thus covers a larger region of the interaction in terms of boundary layer thickness than Model 1. A more detailed description of the experimental geometries is given in Ref. 5.

2.2 Wind Tunnel

The experimental study was carried out in the Princeton University blowdown wind tunnel. The test section has a cross area of 8 inches by 8 inches. The test conditions for the present tests were a Mach number of 2.95, a stagnation pressure of 100 psia, an average stagnation temperature of 472°R and a tunnel wall temperature of 10 to 20% above the adiabatic wall temperature. These test conditions resulted in a Reynolds number per inch of 1.6×10^6 and a maximum test time of 6 minutes. Details of the basic facility are given in Ref. 6.

Previous measurements had indicated that the boundary layer flow over the bottom and top walls were equivalent and planar, two-dimensional. The bottom wall boundary layer was used as the test layer for the Model 1 study. Windows positioned in the top and bottom walls were used either as observation or instrumentation ports. In general, pressure distribution studies were carried out with instrumentation mounted in the bottom window. The top window was used as an observation port for photography of oil flow patterns.

2.3 Surface Measurements

Oil flow studies: A technique developed for the present test conditions used a fluorescent oil applied upstream of the region of study before the tunnel was started. Approximately 10 seconds after the tunnel was operating, photographs were taken of the oil pattern. The particular mixture used consisted of clear motor oil and green fluorescent dye thinned with kerosene. The oil patterns were illuminated by a high intensity ultra violet light source. This particular combination of ultra violet excitation and green fluorescence made it possible to filter out the ultra violet reflections coming from the metal test surface. Good results were obtained under all test conditions.

Surface static pressure: Measurements were made on Model 1 using an instrumented plate which fitted into the bottom window port. A large number of static pressure taps was necessary to map the full flow field involving the interaction and to account for the change in shock location when the shock generator angle was varied. During a test, a fixed shock generator position was held while a scanivalve measured the static pressure distribution. The basic static pressure window port could not be used for Model 2, so the test surface itself was instrumented with an arrangement of static pressure orifices.

Heat transfer: Several techniques were investigated to measure the heat transfer rate over the test area. The method finally chosen was a quasi-transient method using a slug calorimeter since it matched best to the tunnel operating procedures, gave reasonable spatial resolution and is rather simple to manufacture. Figure 3 shows a photograph of the heat transfer plug and the insert which provides the hot air. A line drawing of the slug calorimeter arrangement is given in Fig. 4.

To determine the heat transfer rate from the wall to the gas at uniform wall temperature conditions it is necessary that the test piece (slug) be heated to a temperature higher than the surrounding wall temperature. This heating was provided by impinging a tiny jet of hot air to the inside of each slug calorimeter. After the hot air heating is stopped, the slug would attempt to reach the wall recovery temperature as time progresses. At an intermediate time, t_o, while the slug temperature is dropping it equals to the wall temperature. From an exponential curve fitted to the measured slug temperature-time data points, the temperature-time gradient was evaluated at t_o. The convective heat transfer follows from this temperature-time derivative and the calorimeter properties. Heat conduction from the slug to the surrounding wall was minimized by separating the slugs from the aluminum plug by nylon insulation. It was determined that no correction due to insulation losses were necessary.

Skin friction: The Preston tube was used to get some indication of the skin friction. As the present problem involves both pressure gradients and cross flows, there will be uncertainties in the results, particularly for the case of large cross flows. The Preston probe was first aligned with the surface oil flow direction, then rotated 10° in both directions. Although the Preston tube reading was relatively insensitive to such rotation, the largest measured value was used to evaluate the skin friction. The calibration scheme proposed by Bradshaw[7] was used to evaluate the skin friction. He extended the subsonic calibration equation to compressible flow in an alternate way. Instead of using calibration factors to transform to the subsonic calibration coordinates, he added a compressibility correction function to the subsonic calibration equation. This new function has variables which are based upon wall conditions only.

2.4 Flow Field Measurements

To carry out detailed flow field measurements in the interaction region, a probe drive system with two degrees of freedom was used. It moved the probes normal to the wall and yawed them. The probes themselves were supported by a streamlined section which extended from the top wall down towards the bottom wall boundary layer where the measurements were taken.

Pitot-yaw surveys: To determine the flow angles in the X-Y plane throughout the flow field, a cobra probe has been employed. The cobra probe was traversed and yawed in such a way that the two side pressures remained equal so that the flow yaw angle and pitot pressure could be determined at the same time.

Static pressure surveys: Since it was clear that significant variations in the static pressure would take place within the interaction region, it was necessary to determine the local static pressure in order to evaluate the local flow velocities and density. To obtain a measure of the local values, a small cone-cylinder probe was designed to be used in conjunction with the probe drive mechanism noted previously. The static pressure orifices were located 11 diameters downstream of the tip. The probe rotated in the X-Y plane about the orifice location and was kept aligned with the known flow direction. A calibration of the angle sensitivity of the probe in uniform flow was performed and it was found that over $\pm$ 4°, the static pressure varied less than 2% from the correct value.

Total temperature surveys: To complete the measurements from which the local velocities can be obtained, measurements were made of the total temperature throughout the interaction region. Although the wall temperature was approximately 15% above its adiabatic value, the measurement of small variations of total temperature provide for increased accuracy of the deduced flow field data. The probe used was a fine wire probe which had a thermocouple junction in the middle of the wire. This thermocouple consisted of the junction between alumel and chromel wires which had a thickness of 0.002 inches diameter.

A more detailed description of the experimental techniques used is given in Ref. 5.

3. INCOMING BOUNDARY LAYER CHARACTERISTICS

The boundary layers that interacted with the shock wave were surveyed extensively and were shown to be two dimensional across the width of the wind tunnel. It should be noted, however, that the upstream boundary of the interaction region, as determined from the start of the wall static pressure increase, is a swept line which is approximately parallel to the shock wave. This results in a variation in thickness of the boundary layer coming into the interaction region since the boundary layer is growing in the streamwise direction. The boundary layer that interacted with the shock wave in the Model 1 configuration originated from the tunnel nozzle and increased in thickness from 0.52 to 0.58 inches along a typical interaction region for a 10 degree shock generator angle. The boundary layer for Model 2 was generated on a flat test plate which spanned the tunnel and was located 2 inches above the tunnel bottom wall. The corresponding increase in thickness of this thinner Model 2 boundary layer was much larger because of its shorter running length and amounted to a variation of 0.11 to 0.16 inches. These increases of the incoming boundary layer thickness along the shock wave have to be taken into account when the scale of the interaction length is evaluated in terms of a local boundary layer thickness.

Boundary layer parameters derived from the measurements are tabulated for two typical initial profiles for Model 1 and 2, respectively:

	δ(inches)	δ^*(inches)	θ(inches)	C_f	Re_{inch}
Model 1	0.540	0.162	0.052	0.00119	1.6×10^6
Model 2	0.132	0.040	0.008	0.00150	1.6×10^6

The corresponding velocity profiles were transformed to the incompressible law of the wall variables by using the van Driest transformation as given in Ref. 8. These profiles are then compared with the incompressible wall-wake law as given by

$$\frac{u_{inc}}{u_\tau} = \frac{1}{k} \ln \left(\frac{y u_\tau}{\nu_w}\right) + C + \frac{\Pi}{k} W \left(\frac{y}{\delta}\right) \qquad (1)$$

where $W(\frac{y}{\delta}) = 1 - \cos(\pi \frac{y}{\delta})$, $C = 5.0$, $k = 0.41$, $\Pi = 0.52$.

The comparison (see Fig. 5) shows that the test boundary layers can be described as fully developed, "equilibrium", turbulent boundary layers.

The overall size of the region of study for both Model 1 and 2 in terms of boundary layer thickness is represented in Fig. 6 and compared with those of previous studies by McCabe, Lowrie and Token. Model 1 provides results in an area which is also covered by McCabe and Lowrie, but outside the region studied by Token. Model 2 covers a larger range not heretofore explored.

The general coordinate system used in obtaining and presenting the data is also shown in Fig. 6. The shock location, calculated from the oblique shock theory, is used as the origin for the X_s coordinate.

4. ANALYSIS OF RESULTS AND DISCUSSION

4.1 Three-Dimensional Separation

The notion of flow separation on planar surfaces in both two-dimensional as well as three-dimensional flow is that a boundary layer, flowing tangentially alongside a solid surface, breaks away from this surface due to an adverse pressure gradient. In planar, two-dimensional flows the customary definition of separation requires that the mean wall shear stress vanishes at the separation point. This definition is quite satisfactory for such cases as it implies the start of flow reversal. In three-dimensional flow, however, the situation is more complicated, illustrated by the fact that three-dimensional separation has a two-fold mechanism (see Lighthill, Ref. 9). This mechanism is explained by using the concept of limiting surface streamlines (or skin friction lines). If one considers a streamline at a small distance from the surface, then it follows from the continuity equation that this streamline has to depart from the surface not only in case of vanishing wall shear-stress, but also in a case where the topography of the limiting

surface streamlines is such that they converge. They can coalesce and form a line of ordinary separation. Although the notion of flow separation as applied to two- or three-dimensional flow is the same, the main mechanism through which flow separation takes place can be different; for example, three-dimensional flow can separate from the wall along a separation line without the mean surface shear stress becoming zero. This type of flow separation is known as ordinary separation (see Maskell, Ref. 10) and has to be distinguished from singular separation whose main characteristic is that the mean wall shear stress vanishes at the separation point.

In applying these ideas of flow separation to the present problem, previous investigators have proposed several ways in which the onset of flow separation, over any region of significant size, can be determined from surface flow patterns. The main characteristic of a line of ordinary separation is the tangential convergence of the surface streamlines into one single line. Maskell proposed that the order of magnitude of the rate of this convergence be the same on each side of the separation line. Rogers and Hall[11] have relaxed this criterian for separation, by suggesting that for the condition of incipient separation the limiting surface streamlines converge toward the separation line only in the upstream region, immediately downstream they are parallel to it and further downstream they turn progressively away from it.

Although these criteria of ordinary flow separation are based upon limiting surface streamlines, and thus have to be verified by actual flow field measurements, they are believed to be physically correct. Care, however, must be taken in applying these criteria especially in turbulent boundary layers where the equivalence between limiting surface streamlines (skin friction lines) and oil flow lines is not an obvious matter. In the following sections, there are several discussions specifically aimed at trying to clarify questions about this ordinary flow separation. Finally, objections will be raised against McCabe's criterion for separation as used in other investigations (Refs. 1-4) of the present problem.

4.2 Surface Flow Patterns

Some results obtained during the oil flow studies are presented in Figs. 7 through 10 with α_G = 4 and 10 degrees for both Model 1 and 2. The oil lines for $\alpha_G = 4^o$ downstream of the calculated shock location are deflected to a maximum angle of about 10^o, which is about twice the shock generator angle but remains well below the shock wave angle. For $\alpha_G = 10^o$ the oil lines turn to angles which are substantially larger than the shock wave angle and coalescence of the oil streaks occurs as a consequence. Special attention should be paid to the difference in scale of an average boundary layer thickness between Model 1 and 2. Because of this large region of Model 2 (see Fig. 6) there emerges an area downstream of the shock wave for $\alpha_G = 10^o$ where the oil streak lines are parallel to the shock generator again. This region (II) is indicated on Fig. 10.

The interpretation is that the interaction is completed and the boundary layer has again reached a planar, two-dimensional character in this area indicated. The implication of this observation is that, for example, in the case of $\alpha_G = 10^o$, Y = 2.25 inches, it takes about 30 boundary layer thicknesses downstream of the shock wave before all cross flows have disappeared from the boundary layer. This length of the downstream extent of the interaction has never been observed in previous investigations and is a direct result of the large region covered by Model 2. The fact that the end of the interaction does not appear on the surface flow patterns for α_G smaller than 6^o is an indication that the downstream extent of the interaction in the X-direction is larger for smaller shock generator angles.

These surface flow patterns can be reduced to quantitative data by measuring the angles of local oil lines with respect to the X-direction along a line of Y = constant. Results obtained from that process for shock generator angles ranging from 2 up to 12 degrees are presented in Fig. 11 for Model 2. The theoretical shock wave angles are shown to the left hand side of these figures. From Fig. 11 it can be seen that the rate of decrease of the local oil line angles with distance X_s for small generator angles, $\alpha_G \leq 6^o$, is much smaller than for the larger α_G's . This results in a larger downstream extent for weaker shocks. The explanation of this seemingly contradictory result lies in the topography of the flow field that is associated with the surface flow patterns.

For $\alpha_G = 6^o$ and smaller, the total yaw angles occurring in the flow field remain smaller than the shock wave angle. These flow fields are similar to a classical three dimensional boundary layer flow that negotiates a transverse pressure gradient. This transverse pressure gradient causes the slower moving fluid in the bottom portion of the boundary layer to deflect to larger angles than the faster moving fluid in the outer portion of the boundary layer. This process in which cross flows are produced by the transverse pressure gradient is an instantaneous process or in other words the cross flows are created at the physical location where the transverse pressure gradients are present. These pressure gradients disappear in going downstream of the shock location. The cross flows, however, do not vanish instantaneously, but rather decay slowly. The driving force in this decay process is the magnitude of the cross flow itself. So as the cross flow gets smaller, the rate of decay decreases, and the downstream limit of no cross flow is only reached asymptotically, resulting in very large downstream extent for $\alpha_G \leq 6^o$.

For larger generator angles ($\alpha_G \geq 8^o$) other processes play a role in the decay of cross flows. Since the yaw angles are no longer smaller than the shock angle, it can no longer be considered as regular flow field, but rather a flow with large secondary flows imbedded in it. The fluid in which the large cross flows are produced is transported along the shock direction and thus out of the plane of observation, the X-Z plane. This reorganization process of the flow, as described in a later section on the flow model, causes fluid in which much smaller cross flows are present to pitch down toward the wall resulting in a strong decay of oil line angles with distance X_s for $\alpha_G \geq 8^o$.

McCabe[1] has proposed a simple approximate secondary flow theory. This theory assumes that the limiting streamline angle does not vary with distance downstream of the shock wave. This is an oversimplification of the actual situation as can be seen from Fig. 11. However, if the predicted limiting streamline angle is assumed to be a representation of the maximum of the distribution of oil line angles for a given shock generator deflection, $\alpha_{o_{max}}$, then the theory is a good approximation of the present experimental data, as shown in Fig. 12. The theoretical shock wave angle is also indicated in the figure.

McCabe has also suggested a criterion for ordinary separation which defines the flow as separated if the oil lines are deflected to an angle larger than the shock wave angle. This criterion indicates that the flow is separated for $\alpha_G > 7.5^o$ from the present data (see Fig. 12). The justification of this criterion, however, is very much in question since it would not coincide with the first appearance of an ordinary separation line as shown by McCabe himself. This criterion also implies that the minimum shock generator angle needed for flow separation decreases indefinitely as the shock wave angle decreases with increasing Mach number (see Korkegi, Ref. 12). This last observation indicates that even the practical value of McCabe's criterion is not at all clear.

4.3 Static Pressure Distributions

A typical static pressure distribution is shown in Fig. 13. The distance X_s is normalized by the boundary layer thickness, δ_1 , at the beginning of the pressure rise. The upstream extent of the interaction region measured from the shock position is about 12 δ_1 and largely independent of the shock strength at this station of Y = 2.25 inches of Model 2. The downstream extent is more difficult to define in terms of the static pressure distribution because this limit is reached asymptotically. The observation that the scale of this downstream extent is of the order of 20 to 30 times the incoming boundary layer thickness at Y = 2.25 inches is of quite some significance. This scale was also extracted from the surface flow patterns.

Static pressure distributions obtained along several instrumentation lines of Y = constant were also cross plotted as isobar patterns. A typical isobar pattern is shown in Fig. 14 for $\alpha_G = 10^o$, Model 1. As can be noted, the lines of constant static pressure are approximately parallel to the shock wave and only to a small amount diverging along the shock direction. This indicates that the pressure distribution is quasi-two-dimensional in the sense that this flow quantity is constant in the shock direction to a good approximation.

Some comparison can be made with the data obtained by other investigators. The test conditions are listed in the following table:

	Mach Number	δ_{ave} (inches)	Re_{inch}	$Re_{\delta_{ave}}$
Lowrie (Ref.2)	3.44	0.412	1.02×10^6	4.20×10^5
McCabe (Ref.1)	2.94	0.230	2.06×10^5	0.47×10^5
Token (Ref.3)	3.71	6.0	2.91×10^5	17.5×10^5
Model 1	2.95	0.55	1.6×10^6	8.8×10^5
Model 2	2.95	0.133	1.6×10^6	2.1×10^5

The test Mach number of all these studies is around 3 and the wall temperatures are all near adiabatic. The boundary layer thickness, however, varies by a factor of 40. If the intersection of a line drawn tangent to the maximum slope of a static pressure distribution and the line $\bar{P} = 1$, is taken as the beginning of interaction, then the upstream extent, ΔX , can be defined as the distance between the calculated shock location and this beginning. The upstream extent of the interaction, nondimensionalized by the local incoming boundary layer thickness, is shown in Fig. 15. The Y coordinate in this plot is nondimensionalized by the boundary layer thickness, δ_1 , averaged over the distance between the shock generator leading edge and the station Y = constant considered. This average of δ_1 is indicated by δ_{ave} .

The general agreement of the data in Fig. 15, despite the difference in Mach number and deflection angles, has an important implication. If one recalls that δ_1 varies by a factor of 40, one can reach the conclusion that the boundary layer thickness can provide a basis for scaling parameters in this type of problem.

4.4 Heat Transfer Distribution

The heat transfer results are presented as a nondimensional ratio of the local heat transfer coefficient divided by the flat plate value predicted by the van Driest method[13] for the test conditions upstream of the interaction. It should be noted that the local heat transfer coefficient is defined as the local heat transfer rate nondimensionalized by free stream conditions ahead of the interaction. The wall temperature conditions are uniform throughout the interaction region.

The results indicate, as shown in Fig. 16, that heat transfer rate decreases somewhat as the shock is approached in the streamwise direction, and increases almost linearly with the downstream distance from the shock position. No conclusion about the peak heat transfer could be reached as the maximum occurred at the boundary of the region of study of Model 1. The heat transfer results are also cross plotted as a heat transfer pattern in the X-Y plane and an example is given in Fig. 17 for $\alpha_G = 10^o$, Model 1. The results show a general uniformity of the heat transfer field and demonstrate again the quasi-two-dimensional nature of the interaction region.

4.5 Preston Tube Measurements

The skin friction was deduced from Preston tube measurements taken along Y = 4.0 inches on Model 1 for $\alpha_G = 2^o$ to 10^o. These results of these measurements are shown in Fig. 18 where the skin friction has been nondimensionalized by the upstream flat plate value. The most significant observation is that the skin friction distribution is almost equivalent to the heat transfer distribution. This implies that the Reynolds analogy is valid as a first approximation. If ordinary separation occurs it is not required that the skin friction vanish, therefore, no conclusion about separation can be reached by these results.

4.6 Analysis of Complete Flow Field Data

A complete picture of the mean flow field in the X-Z plane can be constructed from the measured quantities, pitot pressure, yaw angle, static pressure, and total temperature. If the static pressure and the pitot pressure at a point in the field are known, the Mach number can be calculated directly from the isentropic relations for subsonic conditions, and from the Rayleigh Pitot formula in an iterative cycle for supersonic cases. The total energy equation was then applied to give the static temperature and thus the density and u,v velocity components. In addition, the velocity component in the Z-direction, w , can be deduced from the density and u,v velocity distributions by integrating the continuity equation and using the boundary condition $w = 0$ at $z = 0$. Hence

$$w = -\frac{1}{\rho} \int_0^z \left\{ \frac{\partial}{\partial x} (\rho u) + \frac{\partial}{\partial y} (\rho v) \right\} dz' \qquad (2)$$

The derivatives in the integrand were obtained by locally fitting a second order polynomial through three data points followed by a differentiation of the polynomial. Data was taken in one X-Z plane only. To overcome this difficulty of evaluating the $\frac{\partial}{\partial y}$ derivative, the data in the X-Z plane at Y = 4.0 inches was projected along the shock direction to higher and lower values of Y . This procedure assumes that the interaction region is perfectly two-dimensional along the shock direction, but it was found that the resultant w was not sensitive to small changes of the projection direction, e.g., a slight divergence of the projection directions through the interaction. The accuracy of the w component obtained by differentiation and integration of the original data is less than that of u and v . After the w-component is computed, the pitch angle β (defined as $\beta = \arctan(\frac{w}{u})$) can be found. It should be noted that the measurement technique of obtaining u and v is only valid if w remains small compared to $\sqrt{u^2 + v^2}$. This requirement was checked a posteriori and found to be satisfied.

The static pressure distribution in the X-Z plane at Y = 4.0 inches for $\alpha_G = 10^o$, shown in Fig. 19, indicates that within the interaction there is no major region (in terms of δ) where the static pressure is uniform. The flow ahead of the shock is characterized by compression waves extending to well outside the incoming boundary layer. The static pressure field downstream of the shock has a more complicated distribution. The Mach number distribution in this X-Z plane is mostly supersonic, Fig. 20. A shallow subsonic region was measured close to the wall near the shock location.

Large yaw angles are measured in the interaction region (see Fig. 21). The largest yaw angles of 55^o occurred a small distance from the wall and $\overline{X_s} \approx 3$. Despite this small region where the yaw angles are larger than the shock wave angle, there is an extensive region downstream of the shock wave where the yaw angles are substantially less than the shock generator angle ($\alpha_G = 10^o$).

The pitch angle β through the interaction (shown in Fig. 22) provides some additional information. The compression waves ahead of the shock do not only cause increasing yaw angles but also increasing pitch angles. Going through the shock wave these pitch angles don't seem to decrease initially, however, at $\overline{X_s} \approx 3$ rapid changes take place and the pitch angle becomes negative.

In view of the question about ordinary separation, it should be noted from this figure that the pitch angle tends to zero as the wall is approached. This observation is of particular importance at the position ($\overline{X_s} \approx -3$) where the oil lines tend to coalesce. This is the region where one would expect locally large pitch angles. The surveys were taken at stations one boundary layer thickness, δ_1 , apart. Keeping this streamwise resolution in mind it can be concluded that a local coalescence of oil flow lines is not necessarily related to locally large streamline inclination with respect to the wall surface. There is, however, a tendency of the flow to depart from the wall (β positive) but it is uniformly spread out over many boundary layer thicknesses.

4.7 Flow Models and Separation

To depict the flow field in the X-Z plane at Y = 4.0 inches, the following flow model is constructed for $\alpha_G = 10^o$, see Fig. 23. The region A is the undisturbed uniform flow ahead of the interaction with a planar turbulent boundary layer at the wall. The typical character of region B is that it has very slowly increasing yaw angles which remain lower than the shock generator angle ($\alpha_G = 10^o$) even in subregions B_2 and B_3 and only reach the 10^o level far downstream. In region C (the area extending downward from region B and approaching the wall) large yaw angles prevail ($10^o \leq \alpha \leq 55^o$). Yaw angles larger than the shock wave angle ($\alpha_{sh} = 28^o$) occur in subregion C_2. The far flow field downstream of the shock and outside region B contains waves originating from the interaction, region D. The decrease in pitch angles β observed by going from subregion B_2 to B_3 generates expansion waves in the external flow (subregion D_1). Compression waves are present in subregion D_2 where the flow has to turn parallel to the wall again.

The corresponding flow model for $\alpha_G = 4^o$ is also presented, see Fig. 24. The measurements on which this model is based are given in Ref. 5. Unlike the $\alpha_G = 10^o$ case, the yaw angles in this case remain well below the shock wave angle. This means that no reorganization process occurs as in the case of $\alpha_G = 10^o$ where the net transport of fluid along the shock direction incurred negative values of β . Although it was determined that the maximum pitch angles were quite small (1.5^o), they are significantly larger than those associated with boundary layers developing under zero pressure gradient conditions.

It is obvious that for $\alpha_G = 4^o$, although the streamlines are slightly departing from the wall ($\beta \leq 1.5^o$), that there is no question about separation. For the $\alpha_G = 10^o$ case, however, the question of whether the boundary layer should be called separated is not an obvious matter. If one examines the oil flow patterns for $\alpha_G = 10^o$ Figs. 8 and 10) more carefully, the observation can be made that although the oil lines are converging and tend to coalesce upstream of the calculated shock position, they do not converge into one single line. The region in which coalescence occurs is growing in size in the direction

along the shock. This observation is consistent with the idea that the size of the interaction region is increasing with distance along the shock. It is exactly this gradual increase in size that permits the oil lines to converge without incurring locally large pitch angles β corresponding to separation of the flow from the wall. This directly leads to the conclusion that the flow is also unseparated for $\alpha_G = 10^o$.

The results clearly indicate that the qualitative difference between attached flows and flows with ordinary separation for the present problem cannot be taken for granted. The definition of ordinary separation becomes then a matter of some conjecture but does not seem to be as crucial as its counterpart in planar two-dimensional flow concerning singular separation.

5. CONCLUSIONS

A detailed study was carried out of the three-dimensional flow fields caused by the interaction of oblique shock waves and a planar turbulent boundary layer. The main results are the following:

1. Two flow field models have been constructed based on experimental data for shock generator angles of 4^o and 10^o. The measurements give a complete description of the flow fields.

2. Based on the 10^o flow field data, it is concluded that McCabe's criterion for incipient separation is not sufficient to define flow separation.

3. The interaction region is quasi-two-dimensional in an area at sufficient distance from the shock generator. This means that although all three velocity components play an important role, the fluid variables vary only slowly along the shock direction.

4. The heat transfer rate decreases as the shock is approached in the streamwise direction and increases almost linearly with downstream distance from the shock location.

5. Reynolds analogy is valid as a first approximation to the problem.

6. Boundary layer thicknesses will provide a basis for scaling parameters of the upstream extent as a function of the transverse distance Y.

7. The downstream extent of the interaction in X-direction is at least four times as large as the upstream one.

REFERENCES

1. McCabe, A.: "The Three-Dimensional Interaction of a Shock Wave with a Turbulent Boundary Layer", Aeronautical Quarterly, August 1966, pp. 231-252.

2. Lowrie, B. W.: "Cross Flows Produced by the Interaction of a Swept Shock Wave with a Turbulent Boundary Layer", 1965, Ph.D. Thesis, Univ. of Cambridge.

3. Token, K. H.: "Heat Transfer Due to Shock Wave Turbulent Boundary Layer Interaction on High Speed Weapon Systems", 1974, AFFDL-TR-74-77.

4. Neumann, R. D.: "Recent Notes on Interference Heating", 1972, AFFDL-TR-72-12.

5. Oskam, B., Bogdonoff, S. M. and Vas, I. E., "Study of Three-Dimensional Flow Fields Generated by the Interaction of a Skewed Shock Wave with a Turbulent Boundary Layer", 1975, AFFDL-TR-75-21, to be published.

6. Vas, I. E. and Bogdonoff, S. M.: "A Preliminary Report on the Princeton University High Reynolds Number 8" x 8" Supersonic Tunnel", 1971, Internal Memorandum No. 39, Gas Dynamics Laboratory, Princeton University.

7. Bradshaw, P. and Unsworth, K.: Comment on "Evaluation of Preston Tube Calibration Equations in Supersonic Flow", AIAA Journal, Vol. 12, No. 9, September 1974, p. 1293.

8. Hopkins, E. J., et.al.: "Hypersonic Turbulent Skin-Friction and Boundary Layer Profiles on Nonadiabatic Flat Plates", AIAA Journal, Vol. 10, No. 1, January 1972, p. 40.

9. Lighthill, M. J.: "Laminar Boundary Layers", Ch. II, Oxford University Press, Edited by L. Rosenhead, 1963.

10. Maskel, E. C.: "Flow Separation in Three-Dimensions", 1955, RAE-Rp-Aero-2565.

11. Rogers, E. W. E. and Hall, I. M.: "An Introduction to the Flow About Plane Sweptback Wings at Transonic Speeds", J. Roy. Aero. Soc., Vol. 64, 1960, p. 449.

12. Korkegi, R. H.: "A Simple Correlation for Incipient Turbulent Boundary-Layer Separation Due to a Skewed Shock Wave", AIAA Journal, Vol. 11, No. 11, November 1973, p. 1578.

13. Hopkins, E. J. and Inouye, M.: "An Evaluation of Theories for Predicting Turbulent Skin Friction and Heat Transfer on Flat Plates at Supersonic and Hypersonic Mach Numbers", AIAA Journal, Vol. 9, No. 6, June 1971.

ACKNOWLEDGEMENT

This research was supported by the Air Force Flight Dynamics Laboratory, Wright-Patterson Air Force Base, Contract Number F33615-73-C-3133.

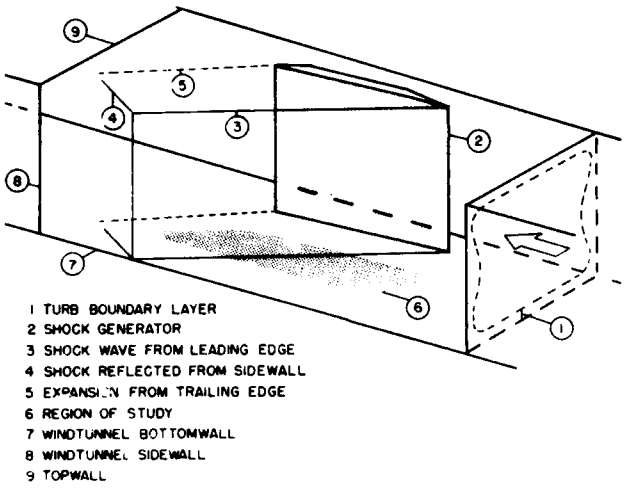

Fig. 1: Schematic of Experimental Configuration

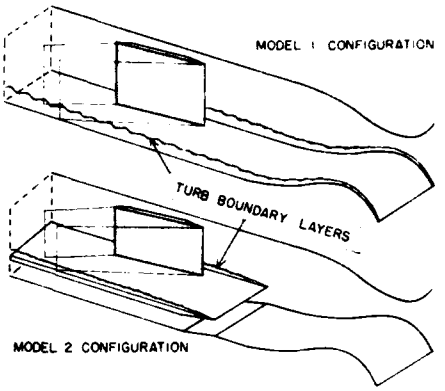

Fig. 2: Model 1 and 2 Configurations

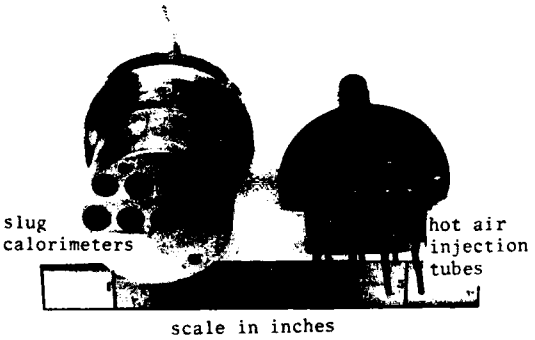

Fig. 3: Heat Transfer Plug

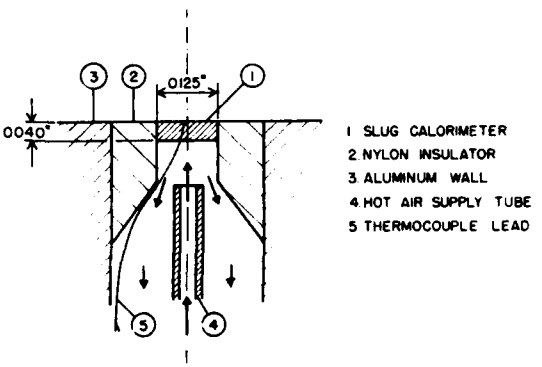

Fig. 4: Slug Calorimeter Arrangement

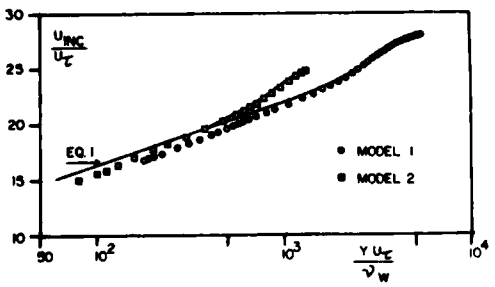

Fig. 5: Transformed Velocity Profiles

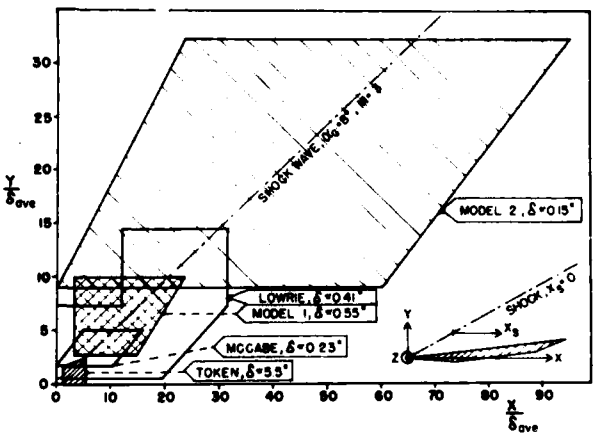

Fig. 6: Regions of Study and Coordinate System

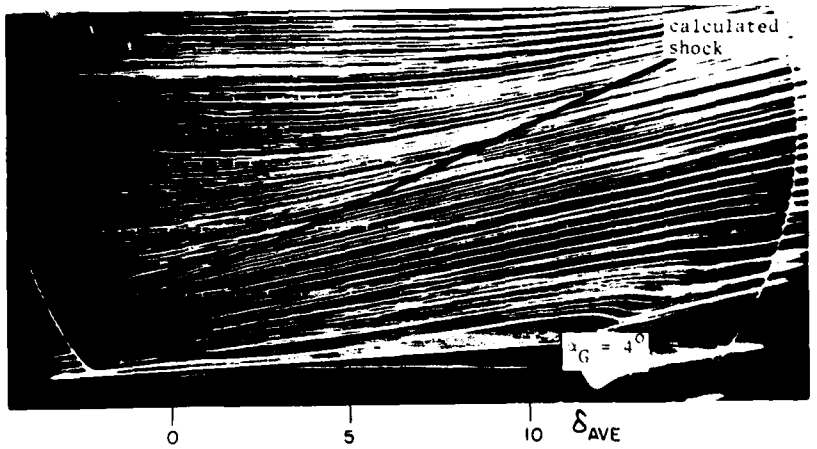

Fig. 7: Photograph of Oil Flow Pattern, $\alpha_G = 4^\circ$, Model 1

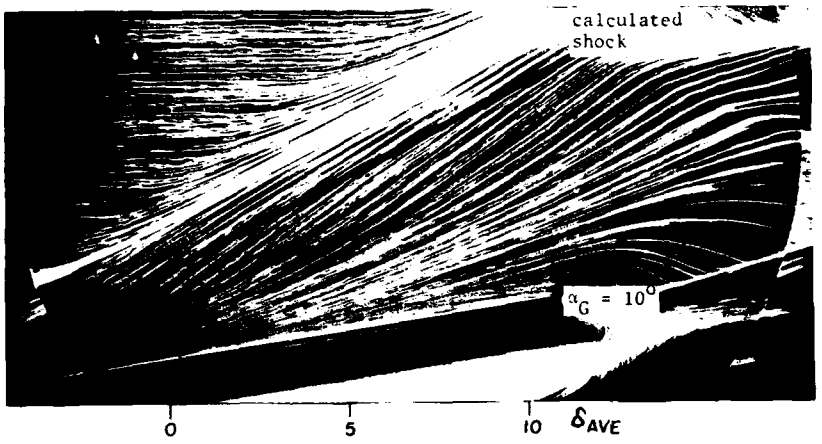

Fig. 8: Photograph of Oil Flow Pattern, $\alpha_G = 10^\circ$, Model 1

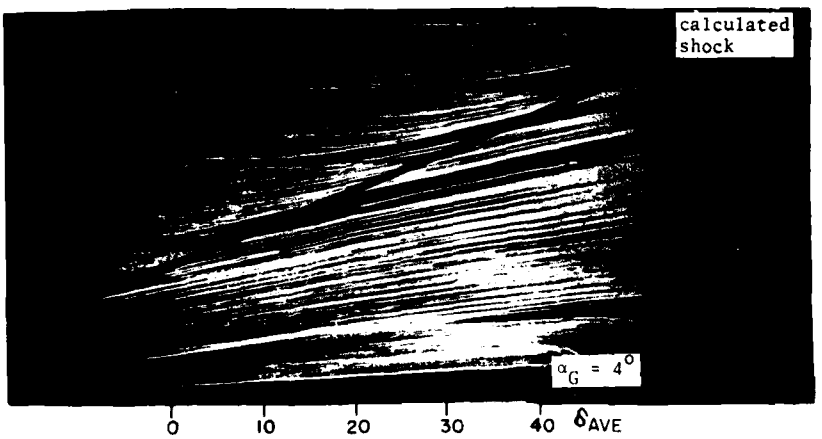

Fig. 9: Photograph of Oil Flow Pattern, $\alpha_G = 4^\circ$, Model 2

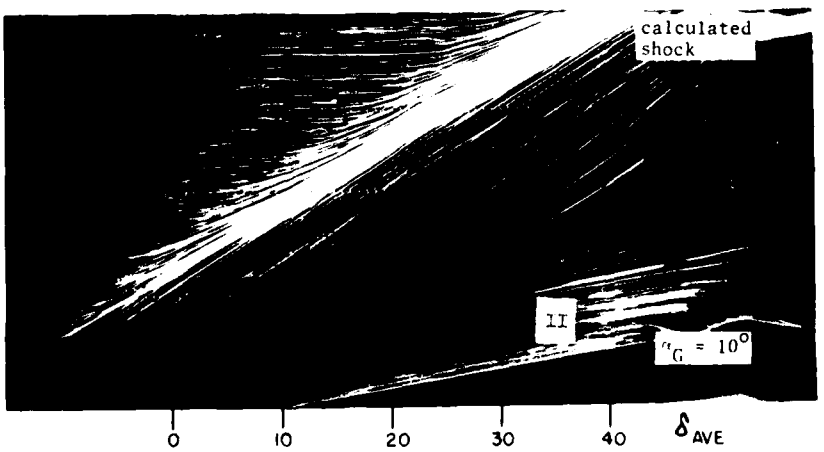

Fig. 10: Photograph of Oil Flow Pattern, $\alpha_G = 10^\circ$, Model 2

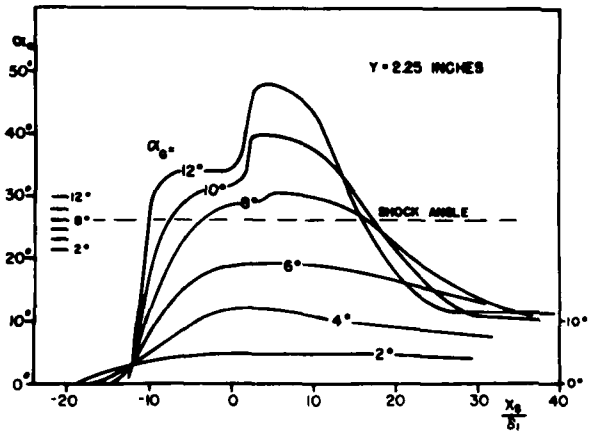

Fig. 11: Oil Line Angles, Y = 2.25 inches, Model 2

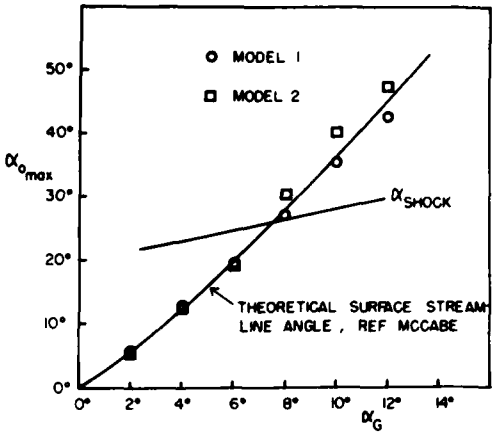

Fig. 12: Comparison with McCabe's Secondary Flow Theory

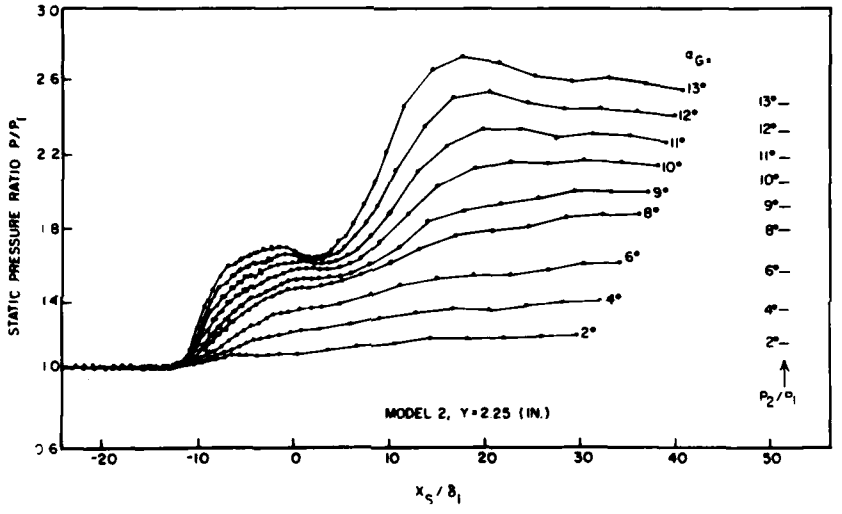

Fig. 13: Static Pressure Distributions, Y = 2.25 inches, Model 2

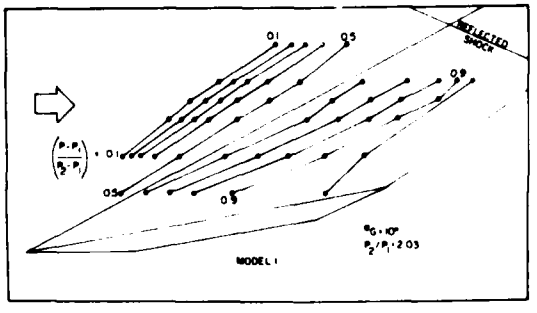

Fig. 14: Surface Isobar Pattern, $\alpha_G = 10^o$, Model 1

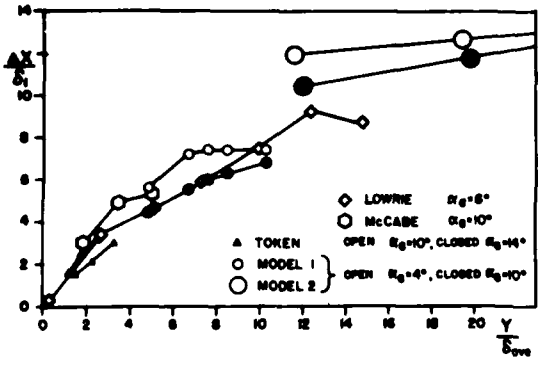

Fig. 15: Upstream Extent of Interaction Region

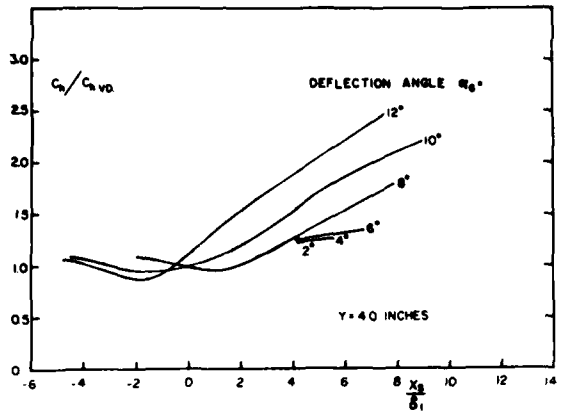

Fig. 16: Heat Transfer, Y = 4.0 inches, Model 1

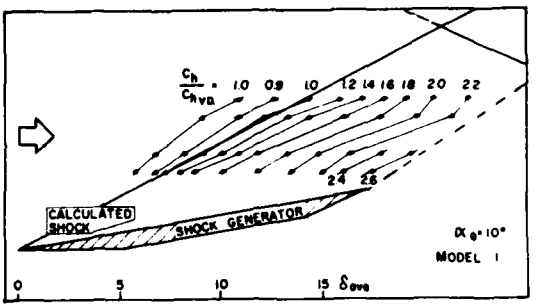

Fig. 17: Heat Transfer Pattern, $\alpha_G = 10^o$, Model 1

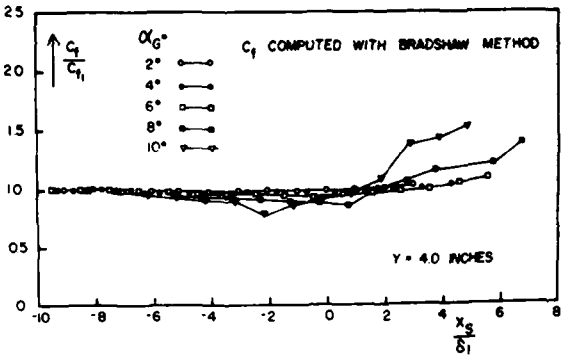

Fig. 18: Skin Friction, Y = 4.0 inches, Model 1

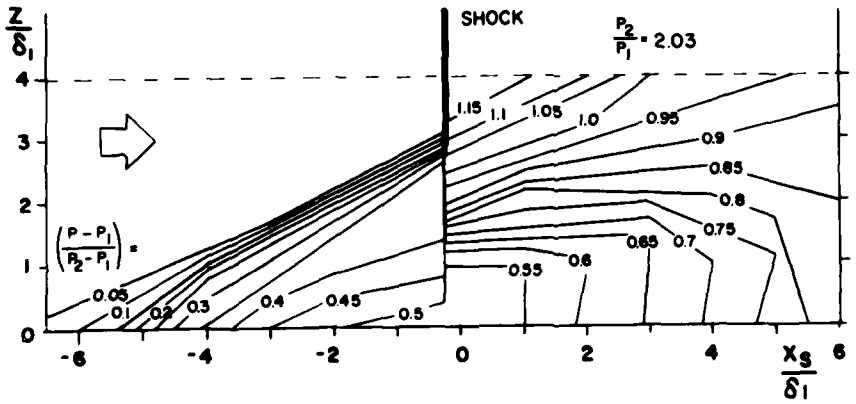

Fig. 19: Static Pressure Contour Plot in XZ-Plane, Y = 4.0 inches, $\alpha_G = 10^o$, Model 1

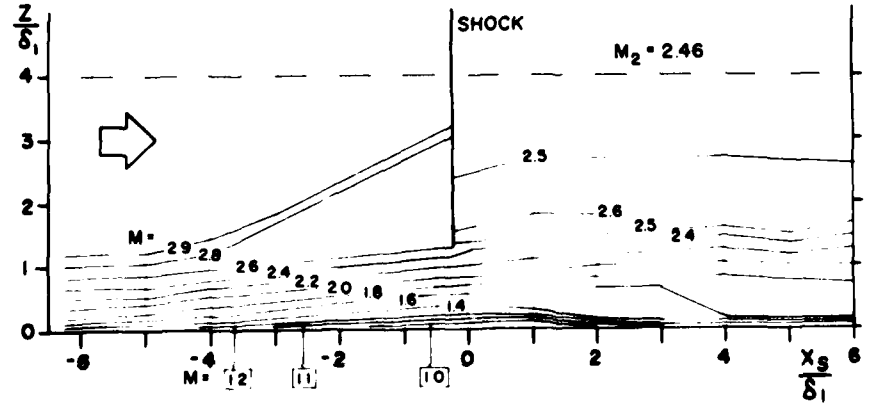

Fig. 20: Mach Number Contour Plot in XZ-Plane, Y = 4.0 inches $\alpha_G = 10^o$, Model 1

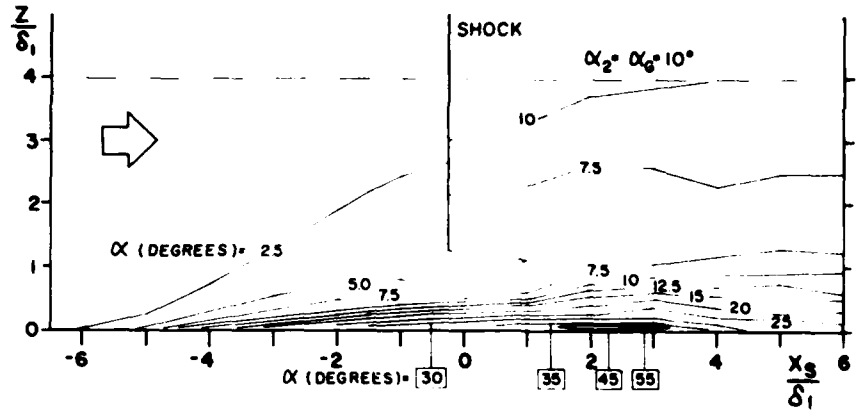

Fig. 21: Yaw Angle Contour Plot in XZ-Plane, Y = 4.0 inches, α_G = 10°, Model 1

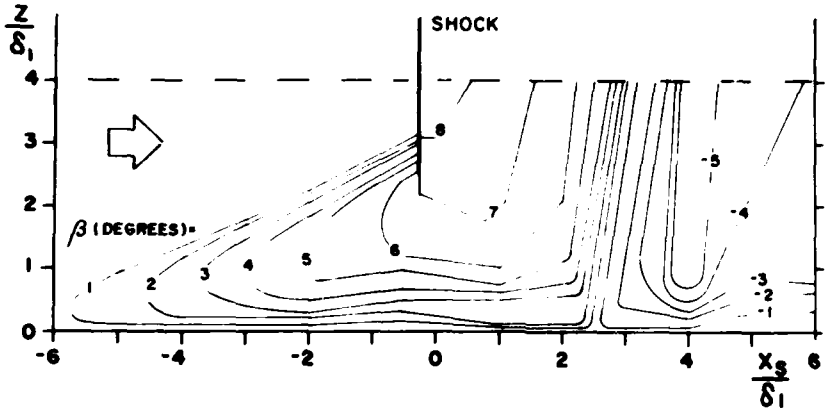

Fig. 22: Pitch Angle Contour Plot in XZ-Plane, Y = 4.0 inches, α_G = 10°, Model 1

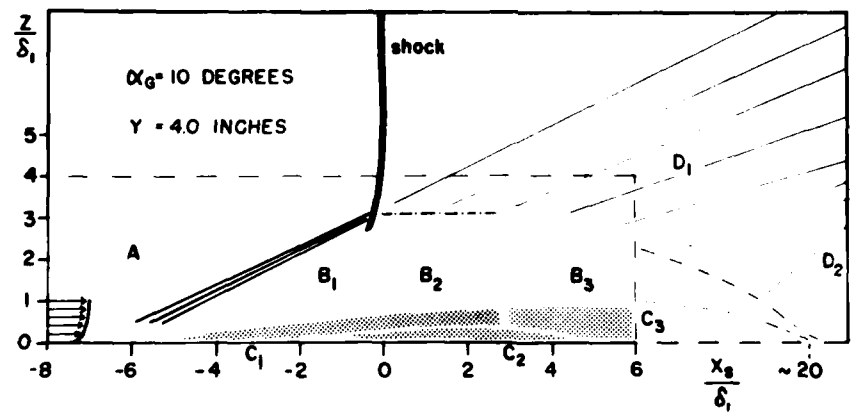

Fig. 23: Flow Model in XZ-Plane, α_G = 10°

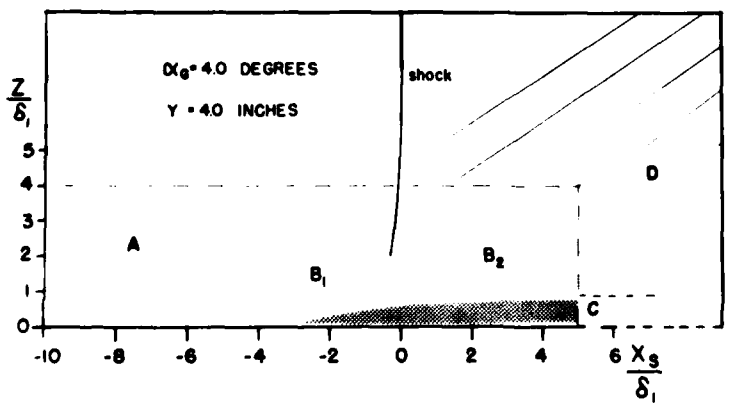

Fig. 24: Flow Model in XZ-Plane α_G = 4°

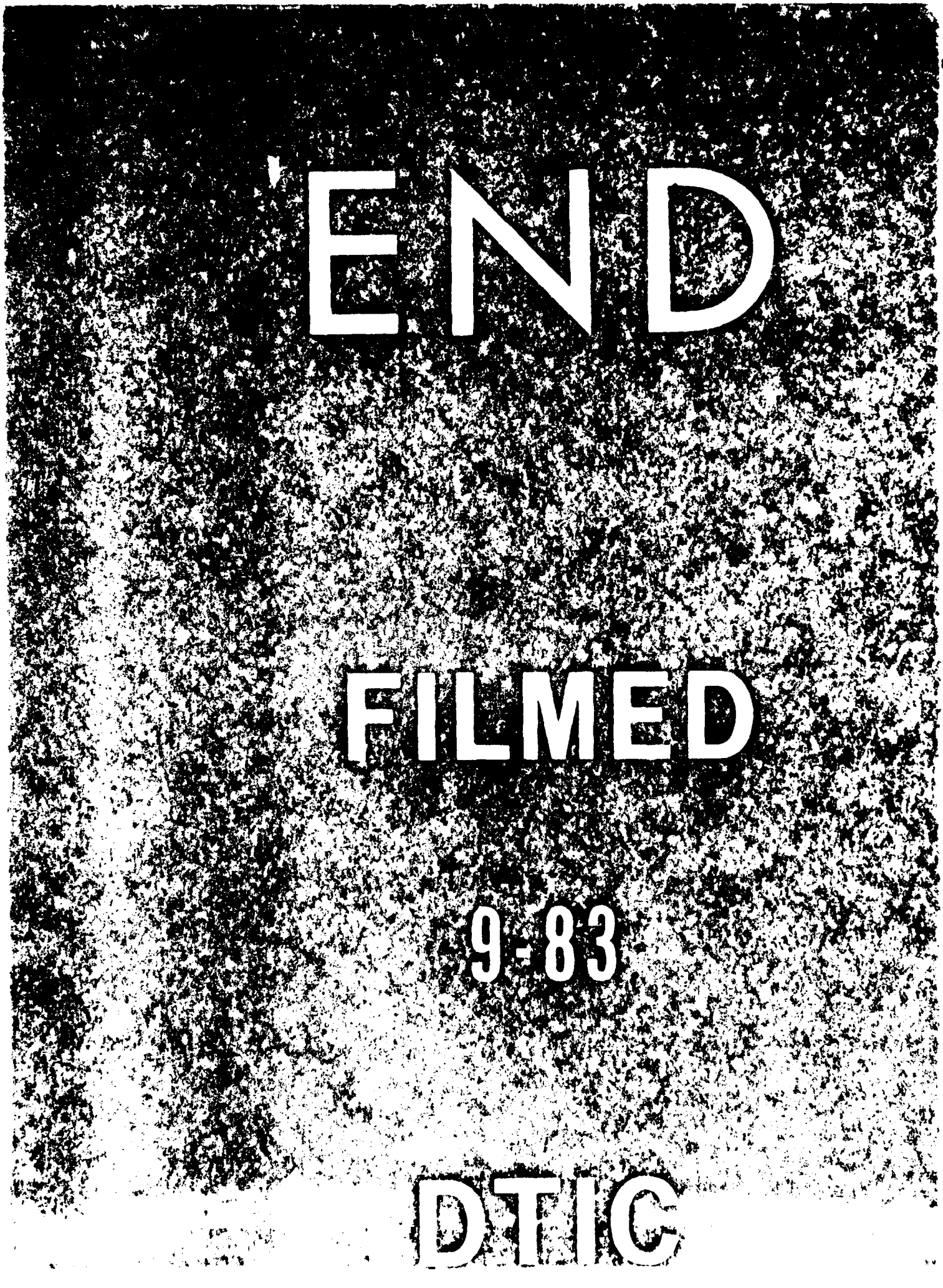
END
FILMED
9-83
DTIC